Metal-Free Cellulose-Based Platforms for Biomolecule Fluorescence Signal Enhancement

Article *in* ACS Sustainable Chemistry & Engineering · December 2021

DOI: 10.1021/acssuschemeng.1c06995

3 authors:

Agata Fularz
University College Dublin
12 PUBLICATIONS **103** CITATIONS
SEE PROFILE

Sawsan Almohammed
University College Dublin
21 PUBLICATIONS **305** CITATIONS
SEE PROFILE

James H. Rice
University College Dublin
131 PUBLICATIONS **1,915** CITATIONS
SEE PROFILE

ACS Sustainable Chemistry & Engineering

pubs.acs.org/journal/ascecg

Research Article

Metal-Free Cellulose-Based Platforms for Biomolecule Fluorescence Signal Enhancement

Agata Fularz, Sawsan Almohammed, and James H. Rice*

Cite This: https://doi.org/10.1021/acssuschemeng.1c06995

Read Online

ACCESS | Metrics & More | Article Recommendations | Supporting Information

ABSTRACT: Fluorescence is a rapid and noninvasive technique for analyte detection. Green, sustainable, and safe materials that enhance the analyte fluorescence signal possess the potential to create new green photonic technologies for medical diagnostics. Here, we report that metal-free cellulose-based substrates can be used as platforms to enhance the fluorescence signal from a model immunoassay as well as a wide variety of molecules by over an order of magnitude. The cellulose-based sensing platforms are cost-effective, biocompatible, robust, and result in a reproducible signal variation as low as 16%. We show that molecules at concentrations as low as 100 nM can be detected on cellulose-based substrates. We attribute the observed enhancement to nanofiber-driven clustering of the analyte molecules, high surface roughness, as well as a charge-transfer process.

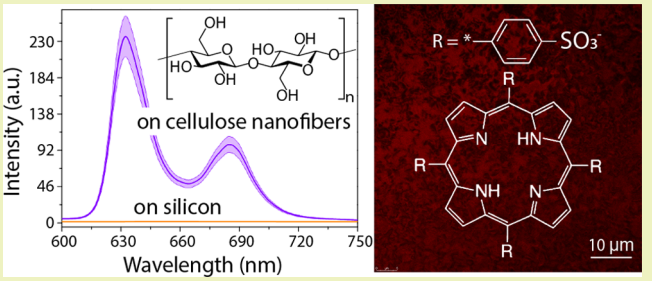

KEYWORDS: *cellulose nanofibers, polymers, enhancement in fluorescence, immunoassays*

INTRODUCTION

The detection of chemical and biological molecules at low concentrations is of critical importance in the fields of medicine, environmental science, food quality analysis, and security.[1−5] Fluorescence spectroscopy is a cost-effective, sensitive, and noninvasive method that is a widely used analytical tool. For example, fluorescence-based detection is used as a readout method for medical immunoassays that are extensively used in diagnosing a wide range of diseases.[6]

A commonly used method to enhance the emission from fluorophores is a technique known as surface-enhanced fluorescence (SEF). It has been shown that plasmon supporting materials such as gold and silver can be used to boost the Raman and fluorescence signal by typically several orders of magnitude when the analyte molecule is positioned in close proximity to the metal (typically 10−90 nm from the surface).[7−10] The use of metal-based templates for the improved detection of biomolecules has several disadvantages; noble metals can be expensive, difficult to manufacture (lithography methods must be used to ensure reproducibility),[11] lack biocompatibility (particularly in the case of silver), and may induce photocatalytic side reactions in analytes.[12] For that reason, fabricating sensing platforms based on dielectric materials that can enhance the fluorescence signal strength from a fluorophore is of enormous interest. Recent work in the field of surface-enhanced Raman spectroscopy (SERS) has demonstrated that various materials such as metal oxide semiconductors,[13−16] as well as graphene and related two-dimensional (2D) layered materials (hexagonal boron nitride (h-BN), MoS_2),[17,18] have been successfully exploited as SERS substrates. This work has extended to the use of metal-free organic polymers[19,20] and peptide-based self-assembling materials.[21] These metal-free organic materials enhance the Raman signal through a combination of effects including surface roughness, wettability as well as charge-transfer-based processes.[19−21] In this work, we address the potential for biomaterial templates for fluorescence signal enhancement.

Cellulose is an organic biopolymer with the formula $(C_6H_{10}O_5)_n$, which consists of β-linked D-glucose units, shown in Figure 1a.[22] As it is the most abundant organic polymer on Earth and can be easily chemically modified, cellulose-based materials have found numerous applications in the field of material science, in particular, in the fabrication of composite materials alternatives to traditionally used plastics.[23,24] Cellulose nanofibers (CNFs) are one-dimensional nanocellulose structures consisting of interlinked amorphous and crystalline cellulose regions with lengths up to several micrometers that can be extracted from wood-derived fibers.[24,25] Cellulose and cellulose-based derivatives[26,27] have been previously used as SERS templates for sensing due to

Received: October 13, 2021
Revised: December 9, 2021

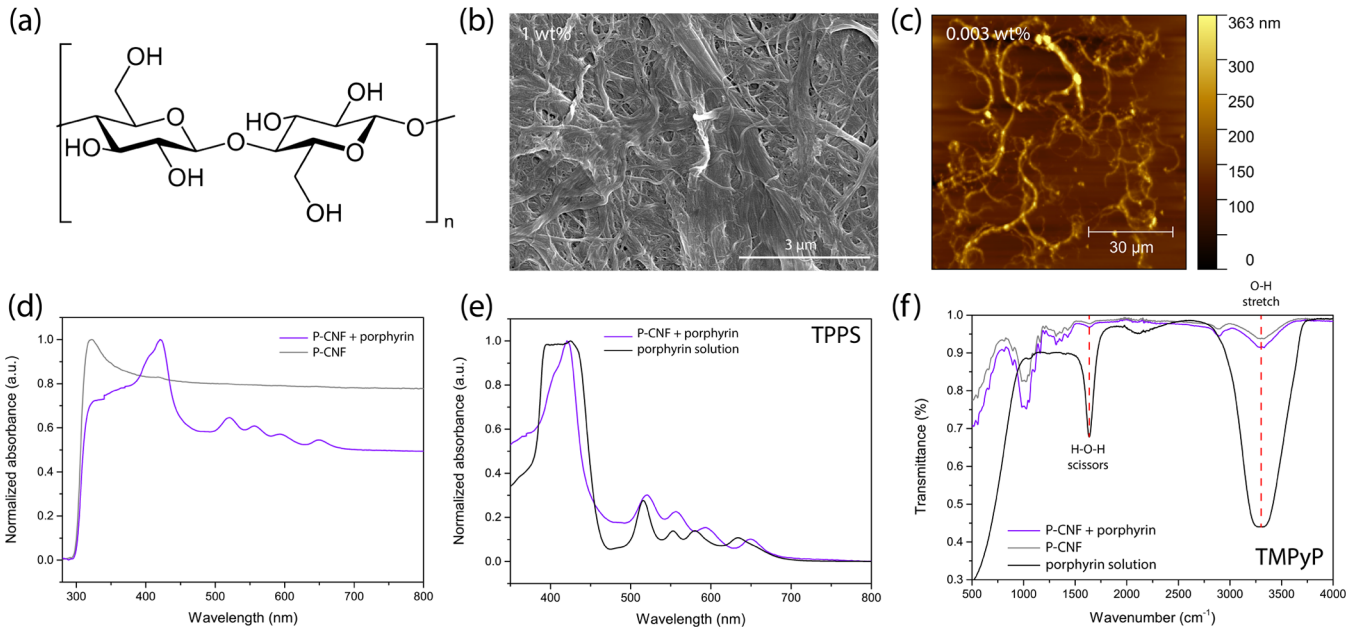

Figure 1. (a) Chemical structure of a cellulose molecule, (b) scanning electron microscopy (SEM) image of highly concentrated pristine cellulose nanofibers (P-CNF) deposited on a silicon substrate, and (c) atomic force microscopy (AFM) image of diluted P-CNF showing individual fibers. Normalized UV−vis absorption spectra of (d) a sample porphyrin molecule (10^{-3} M porphine tetrasodium salt dodecahydrate (TPPS)) deposited on P-CNF compared to (d) the background spectrum of P-CNF, as well as (e) the spectrum of TPPS in solution. Panel (f) shows the Fourier transform infrared (FTIR) spectra of P-CNF compared to the spectrum of a sample porphyrin molecule (10^{-4} M *meso*-tetra(*N*-methyl-4-pyridyl) porphine tetrachloride (TMPyP)) on P-CNF and in solution.

their biocompatibility, roughness, large surface area,[25] flexibility, ability to be functionalized,[26] or loaded with nanoparticles.[24] Paper-based low-cost, fully recyclable sensing platforms have also been developed for the SERS-based detection electrochemical recognition of biomolecules.[28−30] Metal-free cellulose substrate has been shown to be an effective platform for the enhancement of the fluorescence signal of a fluorescein derivative immobilized on its surface. Several mechanisms have been proposed to explain the increased quantum yield, including a reduction in the rotational freedom of phenyl rings, H-bond formation, and the low polarity, which can decrease the probability of photoinduced intramolecular electron transfer.[31] The fluorescence signal of spiropyran appended onto cellulose has also been reported to be enhanced by 1 order of magnitude. It has been suggested that conformational constraints of cavities in the cellulose structure can increase the quantum yield of merocyanine due to the elimination of solvent influence.[32]

Although individual studies on the use of cellulose-based templates for fluorescence signal enhancement of specific molecules have been done, no approach showing that a wide variety of probe molecules can be enhanced using a metal-free biomaterial has been demonstrated. Additionally, we have previously shown that metal-free cellulose nanofibers can be used as substrates for the detection of porphyrin-type molecules via SERS, making cellulose-based platforms promising candidates for fluorescence enhancement.[33] In this study, we show that the fluorescence signal from an extensive range of molecules including important biomolecules can be enhanced. The enhancement factors of molecules deposited on pristine CNF can reach values up to 120 and are comparable to those usually reported for noble metals (1−2 orders of magnitude for silver)[34,35] and can be further boosted by the application of UV light irradiation. We show that by carefully choosing the type of a cellulose-based substrate, the fluorescence signal from a range of analytes, including a model immunoassay, can be enhanced. Cellulose-based sensing platforms have several advantages when compared to traditionally used metal-based templates, such as biocompatibility, recyclability, and inertness, as well as low cost and ease of manufacturing while being comparable with previously studied materials in terms of signal enhancement values and good reproducibility. This approach shows the potential for linking and detection of antibodies, enzymes, and other important biomolecules and the design of substrates for fluorescence-based detection schemes such as lateral flow or paper-based assays.

RESULTS AND DISCUSSION

We studied a range of cellulose-based substrates as platforms for metal-free fluorescence enhancement, with the main focus on pristine cellulose nanofibers (P-CNF). Additionally, cellulose derivatives including 2,2,6,6-tetramethylpiperidine-1-oxyl (TEMPO radical)-oxidized cellulose nanofibers (TEMPO-CNF), cellulose acetate (CA), and hydroxypropyl cellulose (HPC) were investigated. These materials have the same cellulose backbone as pristine cellulose (shown in Figure 1a), with some of the hydroxyl (−OH) groups being partially replaced with carboxyl, acetyl, and $OCH_2CH(OH)CH_3$ groups for TEMPO-CNF, CA, and HPC, respectively. The chemical structure of the cellulose derivative molecules used is shown in Figure S1. The topography of the substrates fabricated using the different materials also varies with pristine and TEMPO-oxidized cellulose forming nanofibers, while CA and HPC are polymers that produce a thin film upon deposition.

The cellulose-based substrates were fabricated by depositing the material previously dispersed in water on silicon. We first imaged the cellulose nanofiber substrate using scanning

https://doi.org/10.1021/acssuschemeng.1c06995
ACS Sustainable Chem. Eng. XXXX, XXX, XXX−XXX

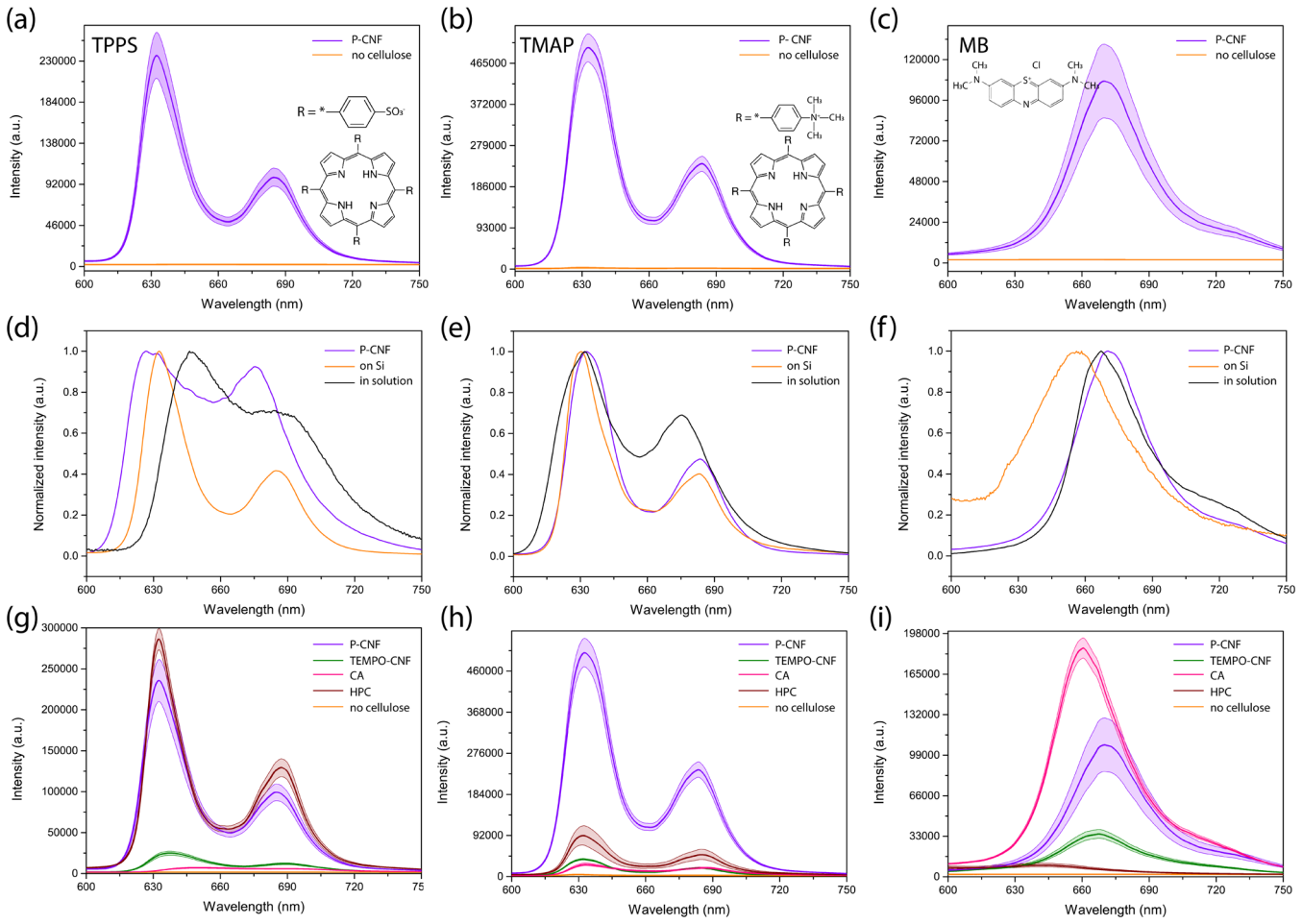

Figure 2. Fluorescence spectra of chosen analyte molecules deposited on P-CNF and drop-cast directly on the Si substrate (a–c), as well as deposited on different types of cellulose derivatives including TEMPO-CNF, HPC, and CA (g–i). Panels (d–f) show the normalized fluorescence spectra of probe molecules in solution compared to analytes deposited on P-CNF and Si, showing the shifts in the position of the peaks. Analyte molecules used were (a, d, g) TPPS, (b, e, h) TMAP, and (c, f, i) MB at concentration 10^{-4} M.

electron microscopy (SEM) and atomic force microscopy (AFM). SEM image (Figure 1b) shows that when highly concentrated P-CNF (1 wt %) is drop-cast on the substrate, a thick layer of randomly oriented fibers occurs with lengths in the range of several micrometers is formed. The diameter of the fibers was determined to be 88 ± 37 nm using a highly diluted dispersion of nanowires deposited on silicon (AFM image shown in Figure 1c; line profiles shown in Figure S3). The fibers seen in the images could be bundles of several smaller elementary cellulose fibrils, which are known to be about 3 nm wide.[36] Figure S2a shows an image of the sample, showing that a white-colored film is produced after drying.

The normalized UV–vis spectrum of P-CNF in Figure 1d shows a broad peak centered around 322 nm, which is consistent with data previously reported in the literature, showing that cellulose absorbs UV light and strongly scatters visible light.[37,38] Upon the addition of a model analyte molecule (porphine tetrasodium salt dodecahydrate; TPPS) to the sample, the peak associated with cellulose becomes less prominent. TPPS is a porphyrin molecule characterized by a high-intensity Soret band and four lower-intensity Q-bands in its UV–vis spectrum.[39] Porphyrins can form J- or H-type aggregates, which can be identified by the observation of red or blue shifts in the UV–vis spectrum, respectively.[40,41] As shown in Figures 1e and S6, most of the porphyrins using the Q-bands become slightly red-shifted following deposition on cellulose, suggesting possible aggregation of the molecules on the cellulose substrate. Since the absorption data provides information about the entire porphyrin adlayer, we may infer that the supporting platform has a large effect on the spatial arrangement of all of the molecules present. For high molecule concentrations investigated in this study, the porphyrin adlayer consists of over 100 individual monolayers (Table S1), suggesting that cellulose in the sample strongly affects the molecule packing, resulting in clustering and aggregation.

Fourier transform infrared (FTIR) spectroscopy spectra of P-CNF compared to the spectrum of a sample porphyrin molecule on P-CNF are shown in Figure 1f. Characteristic peaks of cellulose are observed in the 500–1500 cm^{-1} range, in particular, prominent peaks in the 1030 and 1314–1372 cm^{-1} range can be assigned to C–H bending vibrations,[37,38] while the bands at 1059–1162 cm^{-1} correspond to C–O and C–O–C stretching.[37] A small peak at 897 cm^{-1} is associated with β-glycosidic linkages in the cellulose structure.[42] A broad peak at 1462 cm^{-1} suggests that amorphous cellulose predominates over crystalline cellulose in the sample, which is further confirmed by the low intensity of 750 and 710 cm^{-1} peaks characteristic for Iα and Iβ cellulose allomorphs, respectively.[43] High-intensity broad peaks at 1635 and 3300 cm^{-1} are associated with H–O–H scissors and O–H stretching. The

https://doi.org/10.1021/acssuschemeng.1c06995
ACS Sustainable Chem. Eng. XXXX, XXX, XXX–XXX

intensity of the peaks is greatly reduced upon drying of the sample (Figure S7), which suggests that they are mostly associated with the presence of water molecules in the sample.[44] No additional peaks were observed in the FTIR spectrum after porphyrin was added to the sample.

Cellulose Nanofiber-Enhanced Fluorescence Studies. In the study, we used a wide variety of analyte molecules including porphyrin molecules, dyes, and quantum dots (QDs) drop-cast directly on a layer of highly concentrated pristine cellulose nanofibers, ensuring that the molecule interacts directly with the cellulose surface and not the supporting substrate. Figure 2a−c shows the fluorescence spectra of three chosen molecules TPPS, 5,10,15,20-tetrakis(4-trimethylammoniophenyl)porphyrin tetra(*p*-toluenesulfonate) (TMAP), and methylene blue (MB) deposited on cellulose compared to the signal of the analytes deposited directly on silicon, showing 122-, 132-, and 56-fold enhancement in the fluorescence intensity, respectively. To account for spatial variability, each spectrum is an average signal from 10 different spots on the sample, with the standard deviation indicated by the error bars. The fluorescence spectra of the two porphyrin molecules show two broad bands characteristic for this type of pigment that can be assigned to Q(0,0) and Q(0,1) bands;[40,41] the bands are centered around 647 and 687 nm for TPPS and 633 and 675 nm for TMAP for porphyrin molecules in solution. The fluorescence spectrum of methylene blue in solution is characterized by one broad peak centered around 667 nm, which is consistent with values previously reported in the literature.[45]

Following deposition of the analyte molecules on cellulose, the position of the fluorescence peak shifts, as shown in Figure 2d−f. A shift in the range of 50−400 meV is usually observed between the fluorescence peak of a molecule in the gas phase and the same molecule adsorbed on a substrate. Additionally, depending on the substrate used, red and blue spectral shifts in the fluorescence peak position often accompany fluorescence enhancement or quenching and can be assigned to the formation of H- and J-aggregates due to the coupling of transition dipole moments of neighboring molecules.[46] There is a significant shift in the range of >10 nm in the peak position for molecules deposited on CNF and control samples (summarized in Table S3), which suggests a strong interaction of the cellulose substrate with the analyte molecules.

Figure 2g−i shows the fluorescence spectra of three chosen dyes (TPPS, TMAP, and MB) on different types of cellulose derivative-based substrates including TEMPO-CNF, CA, and HPC. Although different types of cellulose-based materials proved to be the most efficient ones for specific molecules, all of the cellulose derivatives were effective in enhancing the fluorescence signal when compared to the silicon substrate. P-CNF templates were shown to be the most effective cellulose substrate with respect to the enhancement of fluorescence signals for all of the analyte molecules used (Figure S8). The reproducibility of the fluorescence signal obtained for the molecules characterized by the highest enhancement was studied, as shown in Figure S9. Although the cellulose nanofiber-based substrates are relatively rough due to the fibers being distributed randomly, the samples were characterized by a low variation in the strength of the signal generated from different spots of the sample. A relative standard deviation of 17, 16, and 25% was observed for TPPS, TMAP, and MB, respectively.

The wettability of the platforms used was assessed, as it can affect the spreading of the analyte on the surface. Depending on the mechanism, responsible for signal enhancement, hydrophobic substrates may be beneficial, as they would reduce the spreading of the molecule solution prior to drying, resulting in an artificial change of the probe molecule concentration for fluorescence measurements and therefore higher fluorescence intensity.[47] On the other hand, if a direct contact interaction between the substrate and the molecule is responsible for the enhancement, high hydrophilicity of the substrate may also be beneficial, as it would increase the total number of molecules adsorbed. In this study, we are led to believe that lower spreading of the molecule would be advantageous, as a relatively high number of molecules are deposited on cellulose (as outlined in Table S1), resulting in the generation of a thick adlayer with most of the molecules clustering and not being in direct contact with cellulose. As shown in Figure S10, the P-CNF surface characterized by the highest fluorescence enhancement is the most hydrophilic one, with the lowest contact angle of 19.9°, compared to 35.9° for TEMPO-CNF, 82.5° for CA, and 64.1° for HPC. The surface of silicon has a contact angle of approximately 51°. No straight-forward dependence was observed between the measured contact angle and the fluorescence enhancement, as both hydrophobic (P-CNF) and partially wetting (HPC) platforms were characterized by good performance. For that reason, we may assume that the mechanism responsible for the observed enhancement is stronger than any possible effect associated with wettability.

One contributing factor to the observed fluorescence enhancement could be the surface roughness of the different cellulose-based substrates. AFM images of the four different cellulose-based materials along with the calculated root-mean-squared surface roughness are shown in Figure S10. The P-CNF substrate is the roughest surface, followed by CA, TEMPO-CNF, and HPC. The random distribution of cellulose nanofibers in the sample would result in a large number of crevices and grooves that can act like optical cavities amplifying the incident laser light intensity. Dielectric materials shaped into structures with regular nanosized features are known as photonic crystals, and they have previously been shown to be effective at fluorescence enhancement. If a structure is characterized by an optical resonance that matches either the wavelength of the light used for excitation or the light emitted from the fluorophore, then the substrate acts as an optical resonator, resulting in sensitivity enhancements of up to 2 orders of magnitude.[48] Although traditionally highly ordered photonic structures are used, disordered architectures with submicrometer features scatter light to very high proportions, in a process known as coherent multiple light scattering in a random medium. It has been previously shown that randomly distributed cellulose structures such as crystals and nanofibers may trap photons in the air cavities, which has been proposed as a method for the fabrication of random lasers.[49]

Based on the SEM images of the cellulose substrate, previously shown in Figure 1b, we can calculate the size of random cavities in the structure to be in the range of 100−600 nm, which can couple with the laser light used for excitation. Since cellulose does not absorb visible light, the laser light would be reflected toward the adsorbed molecules, resulting in enhanced light absorption and radiative emission. Figure S10e,f shows the specular reflection and absorption spectra of the cellulose derivatives, respectively. The data confirms that the

https://doi.org/10.1021/acssuschemeng.1c06995
ACS Sustainable Chem. Eng. XXXX, XXX, XXX−XXX

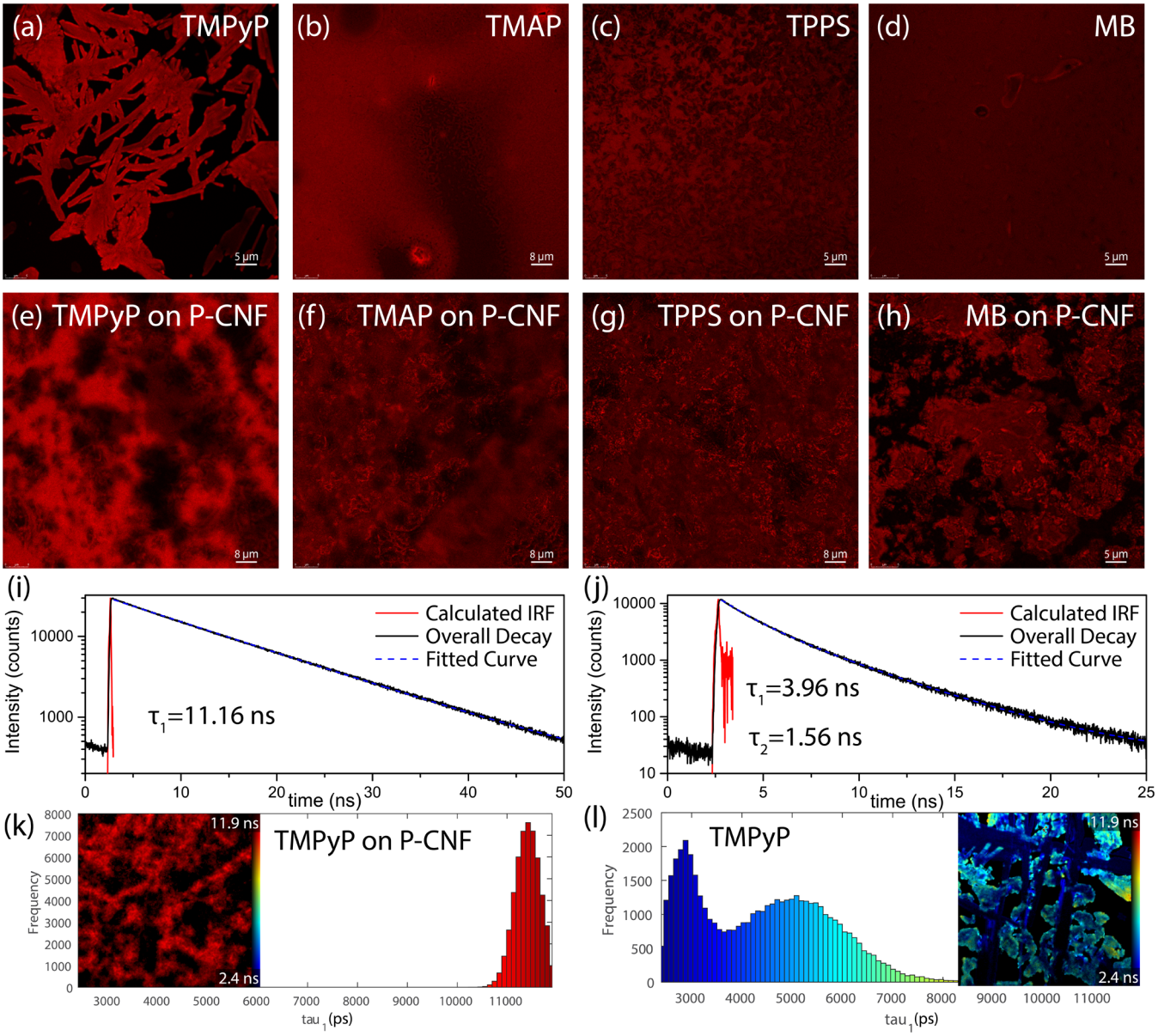

Figure 3. Fluorescence microscopy images of 10^{-3} M (a, e) TMPyP, (b, f) TMAP, and (c, g) TPPS, and (d, h) MB deposited on P-CNF (d, e) and directly on a coverslip (a–c). Fluorescence decay curves along with the lifetimes calculated for (i) TMPyP on P-CNF and (j) TMPyP. Fluorescence lifetime images (FLIM) and the lifetime histograms obtained for (k) TMPyP on P-CNF and (j) TMPyP, respectively. A 532 nm excitation wavelength was used for all of the measurements.

532 nm green laser light is not absorbed by the substrate and the samples are more reflective than glass, although they reflect less light than pure silicon. The light lost could be due to diffuse reflection due to the high roughness of the substrate, resulting in the green light being directed more efficiently toward the molecules adsorbed to the surface.

The fluorescence signal coming from the P-CNF substrate itself is shown in Figure S11a; one low-intensity peak at ∼569 nm can be seen on the spectrum, in agreement with previously reported values in the 500–600 nm range.[50] The different wavelength ranges of the light emitted from the P-CNF and the analyte molecule, as well as the difference in fluorescence signal intensity shown in Figure S11b–d, suggest that the P-CNF background signal does not contribute to the enhancement observed.

Figure 3a–h shows the confocal fluorescence images obtained for chosen fluorophores with and without the presence of cellulose nanofibers. The images outline that there is a significant change in the distribution of molecules on the cellulose surface as the molecules seem to become adsorbed and follow the random arrangement of the fibers. The effect is particularly apparent for *meso*-tetra(*N*-methyl-4-pyridyl) porphine tetrachloride (TMPyP), which is a porphyrin known to self-assemble into nanostructures like nanorods and nanosheets.[51] The images suggest that the self-assembly process is disturbed by the substrate, resulting in the generation of a more disordered adlayer. We have previously investigated the growth and morphology of porphyrin-based adlayers on cellulose surfaces using molecular dynamics simulations based on atomistic empirical force fields in a study published elsewhere.[52] We have shown that molecules

https://doi.org/10.1021/acssuschemeng.1c06995
ACS Sustainable Chem. Eng. XXXX, XXX, XXX–XXX

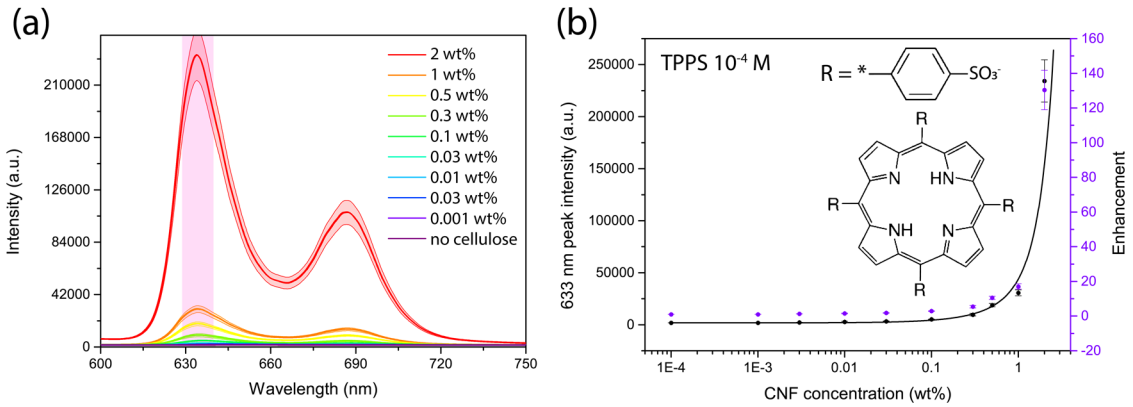

Figure 4. (a) Fluorescence spectrum of 10^{-4} M TPPS deposited on a P-CNF substrate following dilution of the P-CNF dispersion to various concentrations prior to being drop-cast and (b) dependence of the 633 nm peak intensity (black) and the fluorescence enhancement compared to Si-only substrate (purple) on the P-CNF dispersion concentration.

such as *meso*-tetraphenylporphyrin (TPP) and TMPyP form three-dimensional (3D) clusters on the first few relatively ordered layers following the Stranski–Krastanov growth mode, which is consistent with other studies performed on the epitaxial growth of porphyrin-like molecules on organic substrates.[53,54] We can infer that the presence of pristine cellulose nanofibers disrupts the nanostructure assembly process for the porphyrins used in the study, resulting in a generation of a disordered adlayer. The possible clustering of molecules on the substrate could result in an artificial increase of the molecular concentration and therefore the observed fluorescence enhancement.

To better understand the mechanism responsible for the fluorescence increase, fluorescence lifetime microscopy images were collected for chosen analyte molecules deposited on the P-CNF surface. In a typical SEF enhancement process, a decrease in the fluorescence lifetime of a dye is observed when positioned in close proximity to plasmonic nanostructures.[55] A shorter fluorescence lifetime allows the fluorophore to undergo more excitation–de-excitation cycles before photobleaching and is associated with higher fluorescence intensity.[10]

We used fluorescence lifetime imaging (FLIM) by multi-dimensional time-correlated single-photon counting (TCSPC) technique to determine the lifetime of TMPyP with and without the presence of cellulose nanofibers, as shown in Figure 3i–l. The fluorescence lifetimes of TMPyP in aqueous solution were previously determined to be equal to τ_1 = 5.3 ns and τ_2 = 1.7 ns,[56] which is close to the values of τ_1 = 3.96 ns and τ_2 = 1.56 ns obtained for a dry TMPyP layer deposited on a coverslip. The lifetime of the porphyrin increases significantly on P-CNF, reaching a value of τ_1 = 11.16 ns. Values of a radiative lifetime and molar absorption coefficient are inversely proportional to each other according to the Strickler–Berg law.[57] This indicates that the fluorescence enhancement observed may be associated with effects other than radiative lifetime such as the distribution of the fluorophores on the substrate should be used to explain the observed phenomenon.

Figure 4 shows the spectrum of TPPS deposited on a P-CNF substrate following dilution of the P-CNF dispersion to various concentrations prior to being drop-cast on silicon. An exponential decrease in the fluorescence peak intensity is observed when the cellulose concentration is reduced. Even though a thick layer of cellulose nanofibers was shown to be the most effective substrate, single nanowires on silicon diluted down to concentrations as low as 0.1 wt % result in an over 2-fold increase in the fluorescence intensity.

The detection limit of the analytes deposited on P-CNF was determined, as shown in Figure S13, illustrating the normalized spectra of TPPS, TMAP, and MB at different concentrations. When the probe molecular concentration is reduced beyond a certain point, the peak associated with the cellulose background becomes prominent, limiting the applicability of this approach. The data shows, however, that the detection limit is improved by 1 order of magnitude for TMAP and 2 orders of magnitude for MB when compared to fluorescence detection on a silicon substrate. The detection limit on metal-free P-CNF substrate can reach values as low as 10^{-7} M.

Immunoassay Studies Using Cellulose Nanofiber-Enhanced Fluorescence. Fluorescence-based immunoassays are often used to detect nonfluorescent molecules by employing an interaction between them with antigens and antibodies they bind to. Fluorescence immunoassays can be based on the immobilization and detection of a fluorescently labeled molecule on a substrate or on a sandwich format, in which secondary antibodies binding to the nonfluorescent molecules have been labeled.[58] To further expand on our approach of cellulose-based fluorescence detection, we show that the P-CNF substrate can be used as a supporting template for immobilization of Alexa Fluor-conjugated streptavidin, which then enhances the generated signal from the molecule, facilitating its detection. The P-CNF platform can be used as both a metal-free substrate for P-CNF-enhanced fluorescence and a supporting substrate for metal-enhanced fluorescence-based measurements.

We used the P-CNF platform as a substrate for immunoassays utilizing a streptavidin–biotin interaction. The quickly forming bond between streptavidin and biotin is one of the strongest noncovalent interactions known in nature (dissociation constant of about 10^{-14} mol/L) characterized by being unaffected by pH, temperature, or the use of solvents. Streptavidin–biotin systems have been widely used in immunoassays and as systems for linking and detection of antibodies, enzymes, and other proteins.[59] In the aforementioned approach, biotinamidocaproyl-labeled bovine serum albumin (biotinylated-BSA; b-BSA) is deposited directly on the surface of metal nanoparticles.[60,61] BSA binds strongly to metal complexes (silver and gold) as well as glass and forms a complete monolayer[35] and ensures that streptavidin- or avidin-conjugated markers can be immobilized. Fluorophores like the

https://doi.org/10.1021/acssuschemeng.1c06995
ACS Sustainable Chem. Eng. XXXX, XXX, XXX–XXX

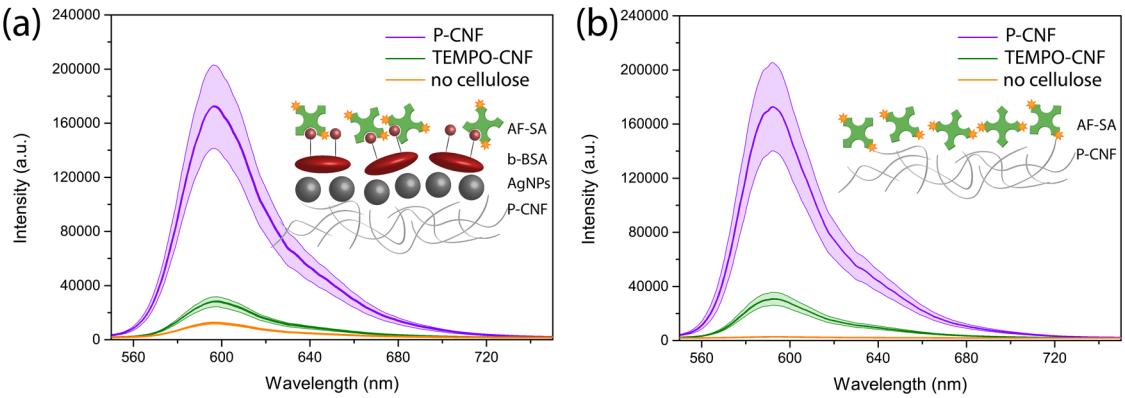

Figure 5. Fluorescence spectra of Alexa Fluor 568 streptavidin (AF-SA)-conjugated dye deposited on (a) b-BSA/AgNPs/CNF and (b) CNF only substrates.

streptavidin-conjugated Alexa Fluor dyes have been attached to metal-based immunoassays resulting in a fluorescence enhancement of ∼2 orders of magnitude for highly ordered silver structures prepared by lithography methods.[35]

Figure 5a shows the fluorescence spectrum of an Alexa Fluor 568 streptavidin (AF-SA)-conjugated dye deposited on an immunoassay consisting of silver nanoparticles (AgNPs) decorated with b-BSA with and without a supporting cellulose nanofiber-based layer. The fluorescence signal is enhanced ∼2-fold when TEMPO-CNF is used and ∼13-fold when P-CNF is used, compared to AgNP-only substrates. AgNPs by themselves have been shown to not influence the fluorescence signal of molecules deposited on cellulose, as outlined in Figure S14, excluding the possibility that the enhancement increases due to localized surface plasmon resonance (LSPR) excitation.

Additionally, the streptavidin-conjugated dye can be directly deposited on cellulose resulting in a similar fluorescence signal intensity observed, as shown in Figure 5b. The AF-SA molecules remain attached to the cellulose nanofibers after the sample is washed with phosphate-buffered saline (PBS). Avidin has been previously shown to easily bind to cellulose modified by carboxyl groups such as TEMPO-oxidated cellulose.[59] Here, however, the highest enhancement was observed for unmodified cellulose, perhaps due to the high surface roughness, inhibiting the removal of AF-SA molecules. The reproducibility of the fluorescence signal of the streptavidin-conjugated dye was studied, as outlined in Figure S16. The full assay consisting of P-CNF, AgNPs, b-BSA, and AF-SA was characterized by a relative standard deviation of 28% when spectra from 30 different, randomly selected spots from the sample were collected. The variation in the signal was 53% for AF-SA directly deposited on cellulose nanofibers. Additionally, we investigated the reproducibility of the signal obtained from different samples, as shown in Figure S17. Six different assays were prepared, and for each, the signal from six different spots of the sample was collected, resulting in a relative standard deviation of 44 and 39% for the full assay with and without P-CNF, respectively. AF-SA deposited directly on P-CNF was the least reproducible signal with 51% relative standard deviation, compared to 11% in signal variability when cellulose was not present. The assays were characterized by a much higher variation in the signal, compared to the previously studied molecules, which may be due to molecule removal following washing of the samples, resulting in less uniform distribution of the dye molecule on the sample. Although the variation in the signal for the assays is significant, it increases only by 5% points when cellulose is added to the full assay, suggesting that most of the signal deviation can be attributed to differences in the adsorption and coverage of b-BSA and AF-SA to the sample and not to the roughness of the supporting P-CNF substrate. Overall, the fluorescence signal of the streptavidin-conjugated dye increased 4.5-fold for the full assay and 53-fold for direct deposition when P-CNF was used as a supporting substrate. The studied assays are robust and allow for molecular detection for a long time following the sample preparation. Figure S18 shows the fluorescence spectra from the full assay obtained from a fresh sample and 6 months following fabrication, showing a high-intensity fluorescence peak, with only a 30% decrease in the signal intensity being observed due to aging.

By developing this model immunoassay, we show that the P-CNF substrate is efficient at immobilization and fluorescence boosting of functionalized streptavidin molecules. Additionally, the assay can be further developed and used for the detection of biotinylated molecules, which can be scavenged from solution by immobilized streptavidin. Immunoassays have been previously employed to detect biotinylated macromolecules, such as thrombin.[62,63] Additionally, similar assays exploring different molecule−antibody interactions can be developed. For instance, influenza-associated HA-antibodies can be detected by labeling them with secondary antibodies conjugated with Alexa Fluor,[64] which opens up opportunities for practical assay development that can be used for medical and clinical diagnostic applications.

Super Band-Gap Irradiation Studies. Lastly, we investigated the effect of irradiating the samples characterized by the highest fluorescence enhancement factor with UV light. Raman signal enhancement has been previously reported for molecules deposited on organic[65] and inorganic[66,67] semiconductor materials following irradiation of the sample with UV light with above-band-gap energy for the given substrate. The enhancement has been assigned to UV-induced photoelectron generation in the substrate and enhanced charge transfer to the analyte molecule. The described mechanism known as photoinduced surface-enhanced Raman spectroscopy (PIERS) was shown to improve limits of detections for SERS. Direct irradiation of fluorophores with UV light has been also previously shown to enhance the fluorescent signal, although the enhancement has been attributed to UV light-driven photochemical reactions of the dyes and not the charge generation in the sample.[68,69] UV irradiation of porphyrins, in

https://doi.org/10.1021/acssuschemeng.1c06995
ACS Sustainable Chem. Eng. XXXX, XXX, XXX−XXX

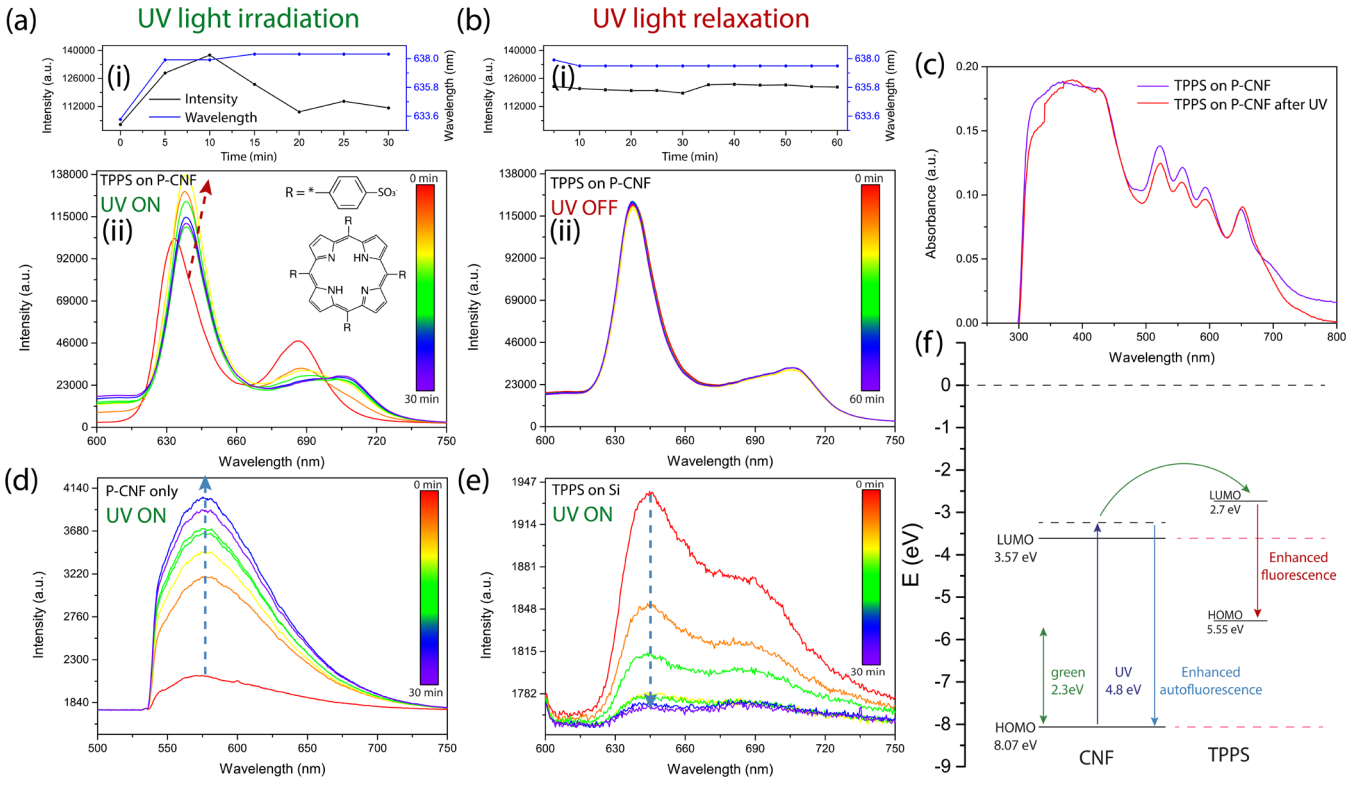

Figure 6. Fluorescence spectrum of 10^{-4} M TPPS on (a-ii) P-CNF substrate for UV light irradiation for up to 30 min and (b-ii) relaxation of the TPPS on P-CNF signal following switching off of the UV lamp. Panels (a-i) and (b-i) show the dependence of the Q(0,0) peak intensity wavelength on the time of UV exposure and relaxation, respectively. The arrows show the change following the UV light exposure and are added to guide the eye. Fluorescence spectrum following UV light irradiation time for (d) P-CNF only and (e) TPPS only. Panel (c) shows the UV−vis spectra of 10^{-4} M TPPS on P-CNF substrate deposited on a coverslip prior to and after UV light exposure. (f) Suggested band diagram explaining the observed fluorescence enhancement.

particular, has been previously shown to quench the fluorescent signal due to photodecomposition and formation of porphyrin derivatives.[70]

Figure 6a shows the fluorescence spectrum of TPPS on P-CNF during the UV irradiation and following a relaxation of the signal. The intensity of the fluorescence signal increases when the lamp is on, with the maximum (1.4-fold increase) being observed after 15 min of irradiation. A red shift in the peak position is also observed when the sample is exposed to UV light. The fluorescence signal remains steady when the light source is removed for at least 1 h (Figure 6b). Figure 6d shows that the signal of the P-CNF-based substrate without an analyte molecule also increases around 2-fold, while the signal of TPPS on silicon substrate decreases due to possible photobleaching effects.[71] No changes were observed in the UV−vis spectrum of porphyrin deposited on cellulose nanofibers prior to and following UV light irradiation (Figure 6e), suggesting that the light exposure does not affect the structure of the layer adsorbed on the cellulose surface.

It can be concluded that the UV light excites charge in the cellulose substrate, resulting in both the enhancement of cellulose autofluorescence and the fluorescence of the analyte molecule deposited on the substrate due to a charge-transfer process taking place. The proposed band diagram explaining the process for TPPS on P-CNF is shown in Figure 6f. The optical band gap of nanofibrillated cellulose has been previously reported to be 4.5 eV, with its highest occupied molecular orbital (HOMO) level being positioned 8.07 eV below the vacuum level.[72,73] The 253.7 nm UV lamp provides an energy of 4.89 eV and therefore can excite electrons to the lowest unoccupied molecular orbital (LUMO) level of cellulose. Subsequently, the green laser light can drive the charge to the LUMO level of TPPS (2.7 eV below the vacuum level), therefore enhancing the radiative emission rates of both TPPS and CNF.[74]

A charge-transfer process similar to that described above but without the use of UV light could be a contribution to the observed fluorescence enhancement of molecules deposited on P-CNF. Figure S20 shows the summary of the observed enhancements and the shifts in the peak position for all of the molecules used, along with a band diagram explaining a possible route for a charge-transfer process. The green laser light (532 nm, 2.3 eV) used in the measurements does not provide enough energy to drive the charge from the substrate to the analyte molecules; it can, however, excite charge from the HOMO level of the molecule directly to the LUMO level of the cellulose. Charge excitation can then be followed by the electrons being driven to the LUMO level of the molecule, followed by radiative emission. In such a process, the green light could result in charge generation in molecules with a larger HOMO−LUMO gap, such as TPPS, that cannot be excited directly. On the other hand, no clear relationship between the energy levels and the observed enhancement could be distinguished for the different porphyrins and dyes, suggesting other processes contributing to the observed phenomenon.

https://doi.org/10.1021/acssuschemeng.1c06995
ACS Sustainable Chem. Eng. XXXX, XXX, XXX−XXX

Table 1. Summary of the Fluorescence Enhancement Factors Obtained for Different Molecules on the P-CNF Substrate Compared to That of Previously Reported Enhancements Reported in the Literature

molecule	platforms used previously	fluorescence enhancement reported previously	fluorescence enhancement on cellulose
neutral porphyrin (TPP)	peptoid-hybridized silica-coated gold nanoparticle[75]	3.27	2.2
	Ag-polymer core−shell NPs[76]	2.3	
cationic porphyrin (TMAP, TMPyP)	ZnO nanoparticles[77]	6 (TMPyP)	63 (TMPyP)
		∼1 (TMAP)	132 (TMAP)
anionic porphyrin (TPPS, TCPP)	silver nanocavity[78]	∼50 (TCPP)	4.7 (TCPP)
			122 (TPPS)
	plasmonic copper array[79]	89.2 (TCPP)	
methylene blue	gold nanorods[80]	Single-molecule detection	56 (10^{-7} M detection limit)
crystal violet	(PMMA)-coated Au@Ag nanorod arrays[81]	27	55
rhodamine B	Shell-isolated Au nanoparticles[82]	∼4	25
InP/ZnS QDs	PLMA polymer composite films with Au@Ag@SiO_2 nanoparticles[83]	12.9	2.5
Alexa Fluor	nanoparticle-spiked Au pillar arrays[64]	270 (Alexa Fluor 647)	53 (Alexa Fluor 568)
immunoassay	particulate gold films[84]	6 (Alexa Fluor 555 antirabbit immunoglobin G)	4.5 (compared to no CNF) 38 (compared to Si) (b-BSA/ streptavidin-conjugated Alexa Fluor 568)
	silver island film[58]	40 (Alexa Fluor 647 antirabbit IgG)	

CONCLUSIONS

We have demonstrated that cellulose-based substrates, in particular, randomly oriented cellulose nanofibers are efficient metal-free platforms for surface-enhanced fluorescence, which can be used as alternatives to expensive and difficult-to-manufacture plasmonic substrates. We show that the fluorescence signal of a wide variety of molecules including porphyrins, dyes, and quantum dots can be enhanced by up to 2 orders of magnitude following deposition on cellulose. Table 1 shows the summary of the fluorescence enhancement factors obtained for different molecules on the P-CNF substrate, compared to previously reported enhancements reported in the literature. The performance of cellulose-based platforms cannot be easily compared to previously used metal-based templates for surface-enhanced fluorescence due to a large range of substrates, materials, and molecules used as analytes studied. We can, however, conclude that the cellulose-based platforms are comparable in performance to traditionally used SEF templates. The studied P-CNFs are characterized by fluorescence enhancement between 2-fold and 130-fold for different analytes with limits of detection reaching values as low as 10^{-7} M, with additional advantages being the biocompatibility, recyclability, cost-efficiency, and ease of fabrication of the P-CNF substrates.

The approach of using cellulose-based platforms for molecular detection via fluorescence spectroscopy is applicable for different types of cellulose derivative-based substrates, including TEMPO-CNF, cellulose acetate, and hydroxypropyl cellulose. Although the mechanism responsible for the enhancement remains unclear, we can speculate that it results from the combination of processes, specifically the clustering of the molecules generating a higher concentration of fluorophores in certain spots of the sample, the high roughness of the surface consisting of crevices and grooves, which can amplify the laser light and reflect it toward the adsorbed molecules, as well as a charge-transfer process resulting in increased radiative emission rates. Additionally, we exclude the possibility of attributing the enhancement to wettability-related effect, as well as changes of the fluorescence lifetime of the analytes. The fluorescence signal on CNF can be further enhanced by irradiating the samples with UV light. Our studies show that cellulose nanofibers can be used as supporting substrates for metal-based immunoassays utilizing the streptavidin−biotin interaction, showing the potential application for linking and detection of antibodies, enzymes, and other important biomolecules. These results implicate that the approach may be employed in the design of assay-based diagnostic tools, such as cellulose-based lateral flow assays, a technique widely used in medicine.

EXPERIMENTAL SECTION

Sample Preparation. Sigma-Aldrich provided all of the chemicals unless stated otherwise. All chemicals were used directly without any further purification.

Pristine cellulose nanofibers (P-CNF; prepared by a supermass colloider; 30−80 nm width, >100 μm length, 3 wt % in water) and TEMPO-oxidized cellulose nanofibers (TEMPO-CNF; 50 nm width, 0.5−80 μm, 1 wt % in water) were provided by Cellulose Lab. For concentration studies, P-CNF and TEMPO-CNF were diluted in distilled water down to the desired concentration and then sonicated for 20 min using a Fisherbrand FB15046 Ultrasonic Cleaning Bath to ensure a uniform distribution of the fibers.

Cellulose acetate powder (CA; average M_n ∼ 30 000 by gel permeation chromatography (GPC); CAS number: 9004-35-7) was dissolved in acetone at 1 wt % and stirred overnight. Hydroxypropyl cellulose (HPC) powder (average M_w ∼ 100 000; CAS: 9004-64-2) was dissolved in deionized water at 1 wt %. The substrates were then prepared by drop-casting the cellulose (CNF, TEMPO-CNF, CA, or HPC) on a silicon substrate and left to dry.

Preparation of Probe Molecule Solutions. Powders of meso-tetraphenylporphyrin (TPP; CAS number 917-23-7), *meso*-tetra(*N*-methyl-4-pyridyl) porphine tetrachloride (TMPyP; T40125, Frontier Scientific), 5,10,15,20-tetrakis(4-trimethylammoniophenyl)porphyrin tetra(*p*-toluenesulfonate) (TMAP, CAS: 69458-20-4), *meso*-tetra(4-sulfonatophenyl) porphine tetrasodium salt dodecahydrate (TPPS; T40699, Frontier Scientific), and *meso*-tetra(4-carboxyphenyl)-porphine (TCPP; T790, Frontier Scientific) were used. Additionally, the following nonporphyrin molecules were used as analytes: methylene blue (MB; CAS 122965-43-9) and rhodamine B (RhB; CAS 81-88-9), methyl green (zinc chloride salt, ∼85%; CAS:7114-03-6), victoria blue B (VBB; CAS: 2580-56-5), and methyl violet 2B (MV2B; CAS: 8004-87-3).

https://doi.org/10.1021/acssuschemeng.1c06995
ACS Sustainable Chem. Eng. XXXX, XXX, XXX−XXX

Water-soluble porphyrin solutions (TMPyP, TPPS, TMAP, and TCPP) as well as MG, VBB, MV2B, MB, and RhB were prepared by dissolving the powders in distilled water at an initial concentration of 10^{-2} or 10^{-3} M. TPP solution was prepared in dichloromethane (CH_2Cl_2, CAS number: 75-09-2).

All of the probe molecule solutions used were diluted down to a concentration of 10^{-4} M using the solvent they were initially dissolved in. Crystal violet 1% aqueous solution (CAS number: 548-62-9) was diluted in distilled water down to a concentration of 10^{-4} M. InP/ZnS quantum dots (QDs; stabilized with oleylamine ligands, λ_{em} = 650 nm, 5 mg/mL in toluene, 776785) were used without further dilution.

Preparation of Assays. Biotinylated bovine serum albumin (b-BSA; Thermo Scientific Pierce 29130) and streptavidin-conjugated dye, Alexa Fluor 568 conjugate (AF-SA; Molecular Probes S11226), were provided by Fisher Scientific.

To immobilize the dye on the cellulose surface, silver nanoparticles (AgNPs; product code 730807; 40 nm particle size, 0.02 mg/mL in aqueous buffer contains sodium citrate as a stabilizer) were drop-cast on the cellulose in a 1:1 ratio and dried. Subsequently, 20 μL of 2 mg/mL b-BSA solution in distilled water was added to the surface and incubated for 1 h and subsequently rinsed with deionized water to remove unbound proteins. Twenty microliters of 0.1 mg/mL AF-SA solution in phosphate-buffered saline (PBS; Alfa Aesar J62692, 10×, pH 7.6) was then added to the surface, incubated for 2 hours, and then rinsed with PBS to remove any unbound molecules.

Fluorescence Spectroscopy. The measurement was performed using a bespoke fluorescence system consisting of a monochromatic laser (HeNe, ThorLabs) with a beam splitter and a long-pass filter (RazorEdge, Semrock), an inverted optical microscope (IX71, Olympus), a spectrograph (SP-2300i, Princeton Instruments), and a charge-coupled device (CCD) camera (iDus 401, Andor).[9,85−87] A 50× objective was used to focus the laser (532 nm wavelength, 5 mW incident power regulated by an attenuator) and collect the fluorescence signal with an exposure time of 2 s in an accumulation mode (10 accumulations). The CCD camera was calibrated over the spectral window using the Raman spectrum of toluene. To take spatial variability into consideration, an average signal from 10 different spots on the sample was reported. Edmund Optics provided a Short Wave UV Quartz Pencil Lamp (#40-759, 253.7 nm, 4.89 eV, a nominal output power of 4.5 mW/cm^2). The samples were irradiated with UV light in situ in 5 min long increments for up to a total time of 30 min at a 2 cm distance from the lamp. The Raman spectra were collected every 5 min when the lamp was off. Following the irradiation, the relaxation of the signal was measured in 5 min steps up to a total time of 60 min.

UV−Vis Absorption and Reflection Spectroscopy. Optical absorbance measurements were performed using an absorbance spectrometer (V-650, JASCO, Inc.) under the following settings: 1 nm step size, 1 nm bandwidth, and 400 nm/min scan speed across a 190−900 nm range. The measurements were performed for samples deposited on a coverslip or as a solution in a quartz cuvette. LAMBDA 750 UV/vis/near-infrared (NIR) spectrophotometer (PerkinElmer) was used to determine the specular reflectance. Reflectance spectra from the substrates were measured as a function of $\Delta R/R = (R_{sample} - R_{background})/R_{background}$ using an aluminum mirror as a reference. The spectra were obtained in the 180−1000 nm range for a 1 nm step size.

Fourier Transform Infrared Spectroscopy. Fourier transform infrared (FTIR) spectroscopy spectra were collected using an α Platinum Bruker system. To record FTIR spectra, the substrates on a coverslip or in solution were placed onto the attenuated total reflection (ATR) interface. Spectra were collected using transmission mode scanning in the range of 400−4000 cm^{-1}.

Scanning Electron Microscopy. Scanning electron microscopy (SEM) images were obtained using a Regulus8230 scanning electron microscopy system following the coating of the substrates with a 5 nm thick layer of iridium. Additional high-resolution SEM images were collected using a Zeiss ULTRA plus high-resolution and analytical field emission microscope equipped with a GEMINI FESEM column capable of a 1 nm resolution at 15 kV. Samples were imaged and uncoated using SE-2 (secondary electron mode) with an accelerating voltage of 1 kV.

Atomic Force Microscopy. AFM images were obtained using an MFP-3D Asylum Research instrument operating in a tapping mode. Monolithic silicon Tap300Al-G probes with aluminum reflective coating (BudgetSensors) were used to obtain the images. The tips used were characterized by the following specifications: 40 N/m (20−75 N/m) force constant, 300 kHz (200−400 kHz) resonance frequency, and 125 μm (115−135 μm) length. The root-mean-squared surface roughness was calculated using Gwyddion software based on a 20 μm height image of the sample.

Fluorescence Imaging. Fluorescence confocal and fluorescence lifetime microscopy images were obtained using the Leica TCS SP8 confocal system using a white light laser set to 532 nm and an internal HyD GaAsP SMD detector. A 100× oil objective was used, and the samples were imaged through a coverslip in air without the introduction of a mounting medium.

Contact Angle. A contact angle measuring system (Kruss Advance Drop Shape Analyser DSA25E) was used to measure contact angles of droplets of deionized water (Milli-Q) on different substrates.

■ ASSOCIATED CONTENT

Supporting Information

The Supporting Information is available free of charge at https://pubs.acs.org/doi/10.1021/acssuschemeng.1c06995.

Chemical structure of the cellulose derivative molecules (Figure S1); high-resolution SEM images of highly concentrated pristine cellulose nanofibers (Figure S2); line profiles obtained from the height AFM image of diluted P-CNF (Figure S3); high-resolution AFM image of an individual pristine cellulose nanofiber (Figure S4); picture of the dry P-CNF samples (Figure S5); UV−vis absorption spectra of porphyrins (Figure S6); FTIR spectra of P-CNF (Figure S7); fluorescence spectra of the remaining probe molecules (Figure S8); fluorescence spectra for reproducibility studies (Figure S9); contact angle measurements, AFM images, reflectance and absorption spectra of cellulose derivatives (Figure S10); background fluorescence spectra (Figure S11); confocal fluorescence microscopy images (Figure S12); detection limit studies (Figure S13); fluorescence spectra with and without AgNPs (Figure S14); additional fluorescence spectra of immunoassays (Figure S15); immunoassay reproducibility studies (Figure S16); immunoassay reproducibility studies for different samples (Figure S17); immunoassay ageing study (Figure S18); study on the effect of UV light irradiation on TMAP on P-CNF (Figure S19); summary of the fluorescence enhancement and a band diagram (Figure S20); dependence of the porphyrin overlayer coverage on the concentration of the analyte molecule used (Table S1); chemical structure of the different analyte molecules used (Table S2); and values of the shift in the highest fluorescence peak intensity and the fluorescence enhancement obtained for all of the analytes (Table S3) (PDF)

■ AUTHOR INFORMATION

Corresponding Author

James H. Rice − *School of Physics, University College Dublin, Dublin 4, Ireland;* orcid.org/0000-0002-1035-5708; Email: james.rice@ucd.ie

https://doi.org/10.1021/acssuschemeng.1c06995
ACS Sustainable Chem. Eng. XXXX, XXX, XXX−XXX

Authors

Agata Fularz − *School of Physics, University College Dublin, Dublin 4, Ireland;* orcid.org/0000-0001-7794-6177

Sawsan Almohammed − *School of Physics, University College Dublin, Dublin 4, Ireland; Conway Institute of Biomolecular and Biomedical Research, University College Dublin, Dublin 4, Ireland;* orcid.org/0000-0002-5990-5088

Complete contact information is available at: https://pubs.acs.org/10.1021/acssuschemeng.1c06995

Author Contributions

A.F., S.A., and J.H.R. designed the experiments and developed the experimental setup. A.F. and S.A. performed UV−vis measurements and fluorescence microscopy imaging. A.F. carried out sample preparation, fluorescence, FTIR, SEM, AFM, and FLIM measurements. All authors analyzed data, discussed results, and wrote and reviewed the manuscript.

Funding

This publication has emanated from research conducted with the financial support of the UCD School of Physics (SIRAT—Scholarship in Research and Teaching). This work was supported by the Sustainable Energy Authority of Ireland (SEAI).

Notes

The authors declare no competing financial interest.

■ ACKNOWLEDGMENTS

The authors would like to thank Ian Reid for access to SEM, David Browne and Gareth Redmond for access to UV−vis, Aaron Martin and Hans Eckhardt for access to FTIR, and Brian Rodriguez for access to AFM. The authors would like to thank Una Prendergast for assistance with confocal microscopy, Dennis Dowling and Frank Vaughan for contact angle measurements, as well as Aran Rafferty for high-resolution SEM. The authors thank Pietro Ballone for insightful comments and discussions. A portion of microscopy characterization and analysis has been performed at the CRANN Advanced Microscopy Laboratory (AML www.tcd.ie/crann/aml/), Trinity College Dublin. FLIM was performed at the Nano Research Facility in Dublin City University.

■ REFERENCES

(1) Alattar, N.; Daud, H.; Al-Majmaie, R.; Zeulla, D.; Al-Rubeai, M.; Rice, J. H. Surface-Enhanced Raman Scattering for Rapid Hematopoietic Stem Cell Differentiation Analysis. *Appl. Opt.* **2018**, *57*, E184−E189.

(2) Pearman, W. F.; Fountain, A. W., III Classification of Chemical and Biological Warfare Agent Simulants by Surface-Enhanced Raman Spectroscopy and Multivariate Statistical Techniques. *Appl. Spectrosc.* **2006**, *60*, 356−365.

(3) Ahmad, M. H.; Sahar, A.; Hitzmann, B. Fluorescence Spectroscopy for the Monitoring of Food Processes. *Measurement, Modeling and Automation in Advanced Food Processing*; Advances in Biochemical Engineering/Biotechnology; Springer, 2017; Vol. *161*, pp 121−151.

(4) Vikesland, P. J. Surface-Enhanced Raman Spectroscopy (SERS) for Environmental Analyses. *Environ. Sci. Technol.* **2010**, 7749−7755.

(5) van Hoek, A.; Vos, K.; Visser, A. J. Ultrasensitive Time-Resolved Polarized Fluorescence Spectroscopy as a Tool in Biology and Medicine. *IEEE J. Quantum Electron.* **1987**, *23*, 1812−1820.

(6) Hicks, J. M. Fluorescence Immunoassay. *Hum. Pathol.* **1984**, *15*, 112−116.

(7) Desai, D. B. Metal Enhanced Fluorescence in CdSe Quantum Dots by Gold Thin Films. *Phys. Chem. Chem. Phys.* **2013**, *15*, 19537.

(8) Nadolski, K.; Benichou, E.; Tarnowicz-Staniak, N.; Żak, A.; Jonin, C.; Matczyszyn, K.; Brevet, P. F. Adverse Role of Shape and Size in Second-Harmonic Scattering from Gold Nanoprisms. *J. Phys. Chem. C* **2020**, *124*, 14797−14803.

(9) Damm, S.; Fedele, S.; Murphy, A.; Holsgrove, K.; Arredondo, M.; Pollard, R.; Barry, J. N.; Dowling, D. P.; Rice, J. H. Plasmon Enhanced Fluorescence Studies from Aligned Gold Nanorod Arrays Modified with SiO2 Spacer Layers. *Appl. Phys. Lett.* **2015**, *106*, No. 183109.

(10) Lakowicz, J. R.; Geddes, C. D.; Gryczynski, I.; Malicka, J.; Aslan, K.; Lukomska, J.; Matveeva, E.; Zhang, J.; et al. Advances in Surface-Enhanced Fluorescence. *J. Fluoresc.* **2004**, *14*, 425−441.

(11) Lordan, F.; Damm, S.; Kennedy, E.; Mallon, C.; Forster, R. J.; Keyes, T. E.; Rice, J. H. The Effect of Ag Nanoparticles on Surface-Enhanced Luminescence from Au Nanovoid Arrays. *Plasmonics* **2013**, *8*, 1567−1575.

(12) Lan, L.; Gao, Y.; Fan, X.; Li, M.; Hao, Q.; Qiu, T. The Origin of Ultrasensitive SERS Sensing beyond Plasmonics. *Front. Phys.* **2021**, No. 43300.

(13) Rice, J. H.; Fularz, A.; Almohammed, S. Controlling Plasmon-Induced Photocatalytic Redox Reactions on WO3 Nanowire/AgNPs Substrates via Defect Engineering. *J. Phys. Chem. C* **2020**, *124*, 25351−25360.

(14) Fularz, A.; Almohammed, S.; Rice, J. H. Oxygen Incorporation-Induced SERS Enhancement in Silver Nanoparticle-Decorated ZnO Nanowires. *ACS Appl. Nano Mater.* **2020**, *3*, 1666−1673.

(15) Cong, S.; Yuan, Y.; Chen, Z.; Hou, J.; Yang, M.; Su, Y.; Zhang, Y.; Li, L.; Li, Q.; Geng, F.; Zhao, Z. Noble Metal-Comparable SERS Enhancement from Semiconducting Metal Oxides by Making Oxygen Vacancies. *Nat. Commun.* **2015**, *6*, No. 7800.

(16) Wu, H.; Wang, H.; Li, G. Metal Oxide Semiconductor SERS-Active Substrates by Defect Engineering. *Analyst* **2017**, *142*, 326−335.

(17) Xu, W.; Mao, N.; Zhang, J. Graphene: A Platform for Surface-Enhanced Raman Spectroscopy. *Small* **2013**, *9*, 1206−1224.

(18) Kim, G.; Kim, M.; Hyun, C.; Hong, S.; Ma, K. Y.; Shin, H. S.; Lim, H. Hexagonal Boron Nitride/Au Substrate for Manipulating Surface Plasmon and Enhancing Capability of Surface-Enhanced Raman Spectroscopy. *ACS Nano* **2016**, *10*, 11156−11162.

(19) Yilmaz, M.; Ozdemir, M.; Erdogan, H.; Tamer, U.; Sen, U.; Facchetti, A.; Usta, H.; Demirel, G. Micro-/Nanostructured Highly Crystalline Organic Semiconductor Films for Surface-Enhanced Raman Spectroscopy Applications. *Adv. Funct. Mater.* **2015**, *25*, 5669−5676.

(20) Yilmaz, M.; Babur, E.; Ozdemir, M.; Gieseking, R. L.; Dede, Y.; Tamer, U.; Schatz, G. C.; Facchetti, A.; Usta, H.; Demirel, G. Nanostructured Organic Semiconductor Films for Molecular Detection with Surface-Enhanced Raman Spectroscopy. *Nat. Mater.* **2017**, *16*, 918−924.

(21) Almohammed, S.; Rodriguez, B. J.; Rice, J. H. Nucleobase Sensing Using Highly-Sensitive Surface-Enhanced Raman Spectroscopy Templates Comprising Organic Semiconductor Peptide Nanotubes and Metal Nanoparticles. *Sens. Bio-Sens. Res.* **2019**, *24*, No. 100287.

(22) Zhang, K.; Barhoum, A.; Xiaoqing, C.; Haoyi, L.; Samyn, P. Cellulose Nanofibers: Fabrication and Surface Functionalization Techniques. *Handbook of Nanofibers*; Springer, 2019; pp 1−41.

(23) Van Rie, J.; Thielemans, W. Cellulose-Gold Nanoparticle Hybrid Materials. *Nanoscale* **2017**, *9*, 8525−8554.

(24) Xiong, Z.; Lin, M.; Lin, H.; Huang, M. Facile Synthesis of Cellulose Nanofiber Nanocomposite as a SERS Substrate for Detection of Thiram in Juice. *Carbohydr. Polym.* **2018**, *189*, 79−86.

(25) Liou, P.; Nayigiziki, F. X.; Kong, F.; Mustapha, A.; Lin, M. Cellulose Nanofibers Coated with Silver Nanoparticles as a SERS Platform for Detection of Pesticides in Apples. *Carbohydr. Polym.* **2017**, *157*, 643−650.

(26) Kim, D.; Ko, Y.; Kwon, G.; Kim, U. J.; Lee, J. H.; You, J. 2,2,6,6-Tetramethylpiperidine-1-Oxy-Oxidized Cellulose Nanofiber-Based Nanocomposite Papers for Facile in Situ Surface-Enhanced

Raman Scattering Detection. *ACS Sustainable Chem. Eng.* **2019**, *7*, 15640−15647.
(27) Espinha, A.; Dore, C.; Matricardi, C.; Alonso, M. I.; Goñi, A. R.; Mihi, A. Hydroxypropyl Cellulose Photonic Architectures by Soft Nanoimprinting Lithography. *Nat. Photonics* **2018**, *12*, 343−348.
(28) Pereira, M. V.; Marques, A. C.; Oliveira, D.; Martins, R.; Moreira, F. T. C.; Sales, M. G. F.; Fortunato, E. Paper-Based Platform with an in Situ Molecularly Imprinted Polymer for β-Amyloid. *ACS Omega* **2020**, *5*, 12057−12066.
(29) Marques, A.; Veigas, B.; Araújo, A.; Pagará, B.; Baptista, P. V.; Águas, H.; Martins, R.; Fortunato, E. Paper-Based SERS Platform for One-Step Screening of Tetracycline in Milk. *Sci. Rep.* **2019**, *9*, No. 17922.
(30) Ferreira, N.; Marques, A.; Águas, H.; Bandarenka, H.; Martins, R.; Bodo, C.; Costa-Silva, B.; Fortunato, E. Label-Free Nanosensing Platform for Breast Cancer Exosome Profiling. *ACS Sens.* **2019**, *4*, 2073−2083.
(31) Lopez, S. G.; Crovetto, L.; Alvarez-Pez, J. M.; Talavera, E. M.; San Román, E. Fluorescence Enhancement of a Fluorescein Derivative upon Adsorption on Cellulose. *Photochem. Photobiol. Sci.* **2014**, *13*, 1311−1320.
(32) Tian, W.; Tian, J. Synergy of Different Fluorescent Enhancement Effects on Spiropyran Appended onto Cellulose. *Langmuir* **2014**, *30*, 3223−3227.
(33) Fularz, A.; Almohammed, S.; Rice, J. H. SERS Enhancement of Porphyrin-Type Molecules on Metal-Free Cellulose-Based Substrates. *ACS Sustainable Chem. Eng.* **2021**, 16808.
(34) Weitz, D. A.; Garoff, S.; Gersten, J. I.; Nitzan, A. The Enhancement of Raman Scattering, Resonance Raman Scattering, and Fluorescence from Molecules Adsorbed on a Rough Silver Surface. *J. Chem. Phys.* **1983**, *78*, 5324−5338.
(35) Xie, F.; Pang, J. S.; Centeno, A.; Ryan, M. P.; Riley, D. J.; Alford, N. M. Nanoscale Control of Ag Nanostructures for Plasmonic Fluorescence Enhancement of Near-Infrared Dyes. *Nano Res.* **2013**, *6*, 496−510.
(36) Usmani, M. A.; Khan, I.; Gazal, U.; Mohamad Haafiz, M. K.; Bhatk, A. H. Interplay of Polymer Bionanocomposites and Significance of Ionic Liquids for Heavy Metal Removal. *Polymer-Based Nanocomposites for Energy and Environmental Applications*; Woodhead Publishing Series in Composites Science and Engineering; Elsevier Ltd., 2018; pp 441−463.
(37) Vipin, A. K.; Fugetsu, B.; Sakata, I.; Isogai, A.; Endo, M.; Li, M.; Dresselhaus, M. S. Cellulose Nanofiber Backboned Prussian Blue Nanoparticles as Powerful Adsorbents for the Selective Elimination of Radioactive Cesium. *Sci. Rep.* **2016**, *6*, No. 37009.
(38) Hai, T. A. P.; Sugimoto, R. Surface Functionalization of Cellulose with Poly(3-Hexylthiophene) via Novel Oxidative Polymerization. *Carbohydr. Polym.* **2018**, *179*, 221−227.
(39) Fularz, A.; Almohammed, S.; Rice, J. H. Electric Field-Induced Boron Nitride/Silver Nanoparticle Template Discharge for Fluorescence Signal Enhancement. *J. Appl. Phys.* **2020**, *128*, No. 213105.
(40) Khairutdinov, R. F.; Serpone, N. Photoluminescence and Transient Spectroscopy of Free Base Porphyrin Aggregates. *J. Phys. Chem. B* **1999**, *103*, 761−769.
(41) Harsha Vardhan Reddy, M.; Al-Shammari, R. M.; Al-Attar, N.; Kennedy, E.; Rogers, L.; Lopez, S.; Senge, M. O.; Keyes, T. E.; Rice, J. H. Micro- or Nanorod and Nanosphere Structures Derived from a Series of Phenyl-Porphyrins. *Phys. Chem. Chem. Phys.* **2014**, *16*, 4386−4393.
(42) Chen, W.; He, H.; Zhu, H.; Cheng, M.; Li, Y.; Wang, S. Thermo-Responsive Cellulose-Based Material with Switchable Wettability for Controllable Oil/Water Separation. *Polymers* **2018**, *10*, No. 592.
(43) Atykyan, N.; Revin, V.; Shutova, V. Raman and FT-IR Spectroscopy Investigation the Cellulose Structural Differences from Bacteria Gluconacetobacter Sucrofermentans during the Different Regimes of Cultivation on a Molasses Media. *AMB Express* **2020**, *10*, No. 84.
(44) Mojet, B. L.; Ebbesen, S. D.; Lefferts, L. Light at the Interface: The Potential of Attenuated Total Reflection Infrared Spectroscopy for Understanding Heterogeneous Catalysis in Water. *Chem. Soc. Rev.* **2010**, *39*, 4643−4655.
(45) Pahang, F.; Parvin, P.; Ghafoori-Fard, H.; Bavali, A.; Moafi, A. Fluorescence Properties of Methylene Blue Molecules Coupled with Metal Oxide Nanoparticles. *OSA Continuum* **2020**, *3*, 688−697.
(46) Kerfoot, J.; Korolkov, V. V.; Nizovtsev, A. S.; Jones, R.; Taniguchi, T.; Watanabe, K.; Lesanovsky, I.; Olmos, B.; Besley, N. A.; Besley, E.; Beton, P. H. Substrate-Induced Shifts and Screening in the Fluorescence Spectra of Supramolecular Adsorbed Organic Monolayers. *J. Chem. Phys.* **2018**, *149*, No. 054701.
(47) Liu, Q.; Yu, J.; Wang, H. The Role of the Substrate Roughness in Contact Angle Hysteresis and Dynamic Deviation. *Int. J. Heat Mass Transfer* **2020**, *148*, No. 118985.
(48) Mathias, P. C.; Ganesh, N.; Cunningham, B. T. In *Combined Enhanced Fluorescence and Label-Free Biomolecular Sensing with a Two-Dimensional Photonic Crystal*, LEOS 2007—IEEE Lasers and Electro-Optics Society Annual Meeting Conference Proceedings, 2007; pp 71−72.
(49) Reimer, M.; Zollfrank, C. Cellulose for Light Manipulation: Methods, Applications, and Prospects. *Adv. Energy Mater.* **2021**, No. 2003866.
(50) Ding, Q.; Han, W.; Li, X.; Jiang, Y.; Zhao, C. New Insights into the Autofluorescence Properties of Cellulose/Nanocellulose. *Sci. Rep.* **2020**, *10*, No. 21387.
(51) Medforth, C. J.; Wang, Z.; Martin, K. E.; Song, Y.; Jacobsen, J. L.; Shelnutt, J. A. Self-Assembled Porphyrin Nanostructures. *Chem. Commun.* **2009**, 7261−7277.
(52) Fularz, A.; Rice, J. H.; Ballone, P. Morphology of Nanometric Overlayers Made of Porphyrin-Type Molecules Physisorbed on the Surface of Cellulose Iβ Crystals and and Nanocrystals. *J. Phys. Chem. B* **2021**, 11432−11443.
(53) Campione, M.; Hogan, C.; Palummo, M.; Bossi, A.; Yivlialin, R.; Bussetti, G. Close-Packed Arrangements of Flat-On Free-Base Porphyrins Driven by van Der Waals Epitaxy. *Cryst. Growth Des.* **2020**, *20*, 7450−7459.
(54) Djuric, T.; Ules, T.; Gusenleitner, S.; Kayunkid, N.; Plank, H.; Hlawacek, G.; Teichert, C.; Brinkmann, M.; Ramsey, M.; Resel, R. Substrate Selected Polymorphism of Epitaxially Aligned Tetraphenyl-Porphyrin Thin Films. *Phys. Chem. Chem. Phys.* **2012**, *14*, 262−272.
(55) Borrero Landazabal, D.; Meza Olivo, A. A.; Garay Palmett, K.; Salas Montiel, R. Reduction of the Fluorescence Lifetime of Quantum Dots in Presence of Plasmonic Nanostructures. *J. Phys.: Conf. Ser.* **2019**, *1159*, No. 012004.
(56) Teixeira, R.; Serra, V. V.; Paulo, P. M. R.; Andrade, S. M.; Costa, S. M. B. Encapsulation of Photoactive Porphyrinoids in Polyelectrolyte Hollow Microcapsules Viewed by Fluorescence Lifetime Imaging Microscopy (FLIM). *RSC Adv.* **2015**, *5*, 79050−79060.
(57) Strickler, S. J.; Berg, R. A. Relationship between Absorption Intensity and Fluorescence Lifetime of Molecules. *J. Chem. Phys.* **1962**, *37*, 814−822.
(58) Matveeva, E.; Gryczynski, Z.; Malicka, J.; Gryczynski, I.; Lakowicz, J. R. Metal-Enhanced Fluorescence Immunoassays Using Total Internal Reflection and Silver Island-Coated Surfaces. *Anal. Biochem.* **2004**, *334*, 303−311.
(59) Orelma, H.; Johansson, L. S.; Filpponen, I.; Rojas, O. J.; Laine, J. Generic Method for Attaching Biomolecules via Avidin-Biotin Complexes Immobilized on Films of Regenerated and Nanofibrillar Cellulose. *Biomacromolecules* **2012**, *13*, 2802−2810.
(60) Aslan, K.; Zhang, Y.; Geddes, C. D. Sonication-Assisted Metal-Enhanced Fluorescence-Based Bioassays. *Anal. Chem.* **2009**, *81*, 4713−4719.
(61) Aslan, K.; Lakowicz, J. R.; Szmacinski, H.; Geddes, C. D. Metal-Enhanced Fluorescence Solution-Based Sensing Platform. *J. Fluoresc.* **2004**, *14*, 677−679.

https://doi.org/10.1021/acssuschemeng.1c06995
ACS Sustainable Chem. Eng. XXXX, XXX, XXX−XXX

(62) Sorenson, A. E.; Askin, S. P.; Schaeffer, P. M. In-Gel Detection of Biotin-Protein Conjugates with a Green Fluorescent Streptavidin Probe. *Anal. Methods* **2015**, *7*, 2087−2092.
(63) Pol, L.; Eckstein, C.; Acosta, L. K.; Xifré-Pérez, E.; Ferré-Borrull, J.; Marsal, L. F. Real-Time Monitoring of Biotinylated Molecules Detection Dynamics in Nanoporous Anodic Alumina for Bio-Sensing. *Nanomaterials* **2019**, *9*, No. 478.
(64) Park, S. G.; Xiao, X.; Min, J.; Mun, C. W.; Jung, H. S.; Giannini, V.; Weissleder, R.; Maier, S. A.; Im, H.; Kim, D. H. Self-Assembly of Nanoparticle-Spiked Pillar Arrays for Plasmonic Biosensing. *Adv. Funct. Mater.* **2019**, *29*, No. 1904257.
(65) Almohammed, S.; Zhang, F.; Rodriguez, B. J.; Rice, J. H. Photo-Induced Surface-Enhanced Raman Spectroscopy from a Diphenylalanine Peptide Nanotube-Metal Nanoparticle Template. *Sci. Rep.* **2018**, *8*, No. 3880.
(66) Al-Shammari, R. M.; Baghban, M. A.; Alattar, N.; Gowen, A. A.; Gallo, K.; Rice, J. H.; Rodriguez, B. J. Photo-Induced Enhanced Raman from Lithium Niobate on Insulator Template. *ACS Appl. Mater. Interfaces* **2018**, *10*, 30871−30878.
(67) Ben-Jaber, S.; Peveler, W. J.; Quesada-Cabrera, R.; Cortés, E.; Sotelo-Vazquez, C.; Abdul-Karim, N.; Maier, S. A.; Parkin, I. P. Photo-Induced Enhanced Raman Spectroscopy for Universal Ultra-Trace Detection of Explosives, Pollutants and Biomolecules. *Nat. Commun.* **2016**, *7*, No. 12189.
(68) Haruta, O.; Matsuo, Y.; Ijiro, K. Photo-Induced Fluorescence Emission Enhancement of Azobenzene Thin Films. *Colloids Surf., A* **2008**, *313*−*314*, 595−599.
(69) Ran, X.; Wang, H.; Shi, L.; Lou, J.; Liu, B.; Li, M.; Guo, L. Light-Driven Fluorescence Enhancement and Self-Assembled Structural Evolution of an Azobenzene Derivative. *J. Mater. Chem. C* **2014**, *2*, 9866−9873.
(70) De Luca, G.; Pollicino, G.; Romeo, A.; Patanè, S.; Scolaro, L. M. Control over the Optical and Morphological Properties of UV-Deposited Porphyrin Structures. *Chem. Mater.* **2006**, *18*, 5429−5436.
(71) Glass, D.; Cortés, E.; Ben-jaber, S.; Brick, T.; Peveler, W. J.; Blackman, C. S.; Howle, C. R.; Quesada-cabrera, R.; Parkin, I. P.; Maier, S. A. Dynamics of Photo-Induced Surface Oxygen Vacancies in Metal-Oxide Semiconductors Studied Under Ambient Conditions. *Adv. Sci.* **2019**, *6*, No. 1901841.
(72) Simão, C. D.; Reparaz, J. S.; Wagner, M. R.; Graczykowski, B.; Kreuzer, M.; Ruiz-Blanco, Y. B.; García, Y.; Malho, J. M.; Goñi, A. R.; Ahopelto, J.; Sotomayor Torres, C. M. Optical and Mechanical Properties of Nanofibrillated Cellulose: Toward a Robust Platform for next-Generation Green Technologies. *Carbohydr. Polym.* **2015**, *126*, 40−46.
(73) Srivastava, D.; Kuklin, M. S.; Ahopelto, J.; Karttunen, A. J. Electronic Band Structures of Pristine and Chemically Modified Cellulose Allomorphs. *Carbohydr. Polym.* **2020**, *243*, No. 116440.
(74) Pérez-Morales, M.; De Miguel, G.; Bolink, H. J.; Martín-Romero, M. T.; Camacho, L. Soret Emission from Water-Soluble Porphyrin Thin Films: Effect on the Electroluminescence Response. *J. Mater. Chem.* **2009**, *19*, 4255−4260.
(75) Kim, Y.; Kang, B.; Ahn, H. Y.; Seo, J.; Nam, K. T. Plasmon Enhanced Fluorescence Based on Porphyrin−Peptoid Hybridized Gold Nanoparticle Platform. *Small* **2017**, *13*, No. 1700071.
(76) Niu, J.-X.; Pan, C.-D.; Liu, Y.-T.; Lou, S.-T.; Wu, E.; Wu, B.-T.; Zhang, X.-L.; Jin, Q.-Y. Plasmon-Enhanced Fluorescence of Submonolayer Porphyrins by Silver-Polymer Core-Shell Nanoparticles. *Opt. Express* **2018**, *26*, 3489−3496.
(77) Aly, S. M. B.; Eita, M.; Khan, J. I.; Alarousu, E.; Mohammed, O. F. Remarkable Fluorescence Enhancement versus Complex Formation of Cationic Porphyrins on the Surface of ZnO Nanoparticles. *J. Phys. Chem. C* **2014**, *118*, 12154−12161.
(78) Li, W.; Zhang, J.; Zhou, Y.; Zhang, P. Highly Enhanced Fluorescence of Fluorophores inside a Metallic Nanocavity. *Chem. Commun.* **2011**, *47*, 5834−5836.
(79) Sugawa, K.; Tamura, T.; Tahara, H.; Yamaguchi, D.; Akiyama, T.; Otsuki, J.; Kusaka, Y.; Fukuda, N.; Ushijima, H. Metal-Enhanced Fluorescence Platforms Based on Plasmonic Ordered Copper Arrays: Wavelength Dependence of Quenching and Enhancement Effects. *ACS Nano* **2013**, *7*, 9997−10010.
(80) Zhang, W.; Caldarola, M.; Pradhan, B.; Orrit, M. Gold Nanorod Enhanced Fluorescence Enables Single-Molecule Electrochemistry of Methylene Blue. *Angew. Chem., Int. Ed.* **2017**, *56*, 3566−3569.
(81) Sun, J.; Li, Z.; Sun, Y.; Zhong, L.; Huang, J.; Zhang, J.; Liang, Z.; Chen, J.; Jiang, L. Uniform and Reproducible Plasmon-Enhanced Fluorescence Substrate Based on PMMA-Coated, Large-Area Au@Ag Nanorod Arrays. *Nano Res.* **2018**, *11*, 953−965.
(82) Guerrero, A. R.; Aroca, R. F. Surface-Enhanced Fluorescence with Shell-Isolated Nanoparticles (SHINEF). *Angew. Chem., Int. Ed.* **2011**, *50*, 665−668.
(83) Kim, K. S.; Zakia, M.; Yoon, J.; Yoo, S., Il. Metal-Enhanced Fluorescence in Polymer Composite Films with Au@Ag@SiO_2 Nanoparticles and InP@ZnS Quantum Dots. *RSC Adv.* **2019**, *9*, 224−233.
(84) Zhang, J.; Lakowicz, J. R. Metal-Enhanced Fluorescence of an Organic Fluorophore Using Gold Particles. *Opt. Express* **2007**, *15*, 2598−2607.
(85) Almohammed, S.; Oladapo, S. O.; Ryan, K.; Kholkin, A. L.; Rice, J. H.; Rodriguez, B. J. Wettability Gradient-Induced Alignment of Peptide Nanotubes as Templates for Biosensing Applications. *RSC Adv.* **2016**, *6*, 41809−41815.
(86) Damm, S.; Craig Carville, N.; Manzo, M.; Gallo, K.; Lopez, S. G.; Keyes, T. E.; Forster, R. J.; Rodriguez, B. J.; Rice, J. H. Surface Enhanced Luminescence and Raman Scattering from Ferroelectrically Defined Ag Nanopatterned Arrays. *Appl. Phys. Lett.* **2013**, *103*, No. 083105.
(87) Almohammed, S.; Fedele, S.; Rodriguez, B. J.; Rice, J. H. Aligned Diphenylalanine Nanotube−Silver Nanoparticle Templates for High-Sensitivity Surface-Enhanced Raman Scattering. *J. Raman Spectrosc.* **2017**, *48*, 1799−1807.

https://doi.org/10.1021/acssuschemeng.1c06995
ACS Sustainable Chem. Eng. XXXX, XXX, XXX−XXX